Physicochemical and Immunological Assessment of Engineered Pure Protein Particles with Different Redox States

Katelyn T. Gause,[†] Yan Yan,[†] Jiwei Cui,[†] Neil M. O'Brien-Simpson,[‡] Jason C. Lenzo,[‡] Eric C. Reynolds,[‡] and Frank Caruso*[,†]

[†]ARC Centre of Excellence in Convergent Bio-Nano Science and Technology, and the Department of Chemical and Biomolecular Engineering, The University of Melbourne, Parkville, Victoria 3010, Australia and [‡]Melbourne Dental School, Oral Health CRC, The University of Melbourne, Parkville, Victoria 3010, Australia

ABSTRACT The development of subunit antigen delivery formulations has become an important research endeavor, especially in cases where a whole cell vaccine approach has significant biosafety issues. Particle-based systems have shown particular efficacy due to their inherent immunogenicity. In some cases, fabrication techniques can lead to changes in the redox states of encapsulated protein antigens. By employing a uniform, well-characterized, single-protein system, it is possible to elucidate how the molecular details of particle-based protein antigens affect their induced immune responses. Using mesoporous silica-templated, amide bond-stabilized ovalbumin particles, three types of particles were fabricated from native, reduced, and oxidized ovalbumin, resulting in particles with different physicochemical properties and immunogenicity. Phagocytosis, transcription factor activation, and cytokine secretion by a mouse macrophage cell line did not reveal significant differences between the three types of particles. Oxidation of the ovalbumin, however, was shown to inhibit the intracellular degradation of the particles compared with native and reduced ovalbumin particles. Slow intracellular degradation of the oxidized particles was correlated with inefficient antigen presentation and insignificant levels of T cell priming and antibody production *in vivo*. In contrast, particles fabricated from native and reduced ovalbumin were rapidly degraded after internalization by macrophages *in vitro* and resulted in significant T cell and B cell immune responses *in vivo*. Taken together, the current study demonstrates how the redox state of a protein antigen significantly impacts the immunogenicity of the particulate vaccine formulations.

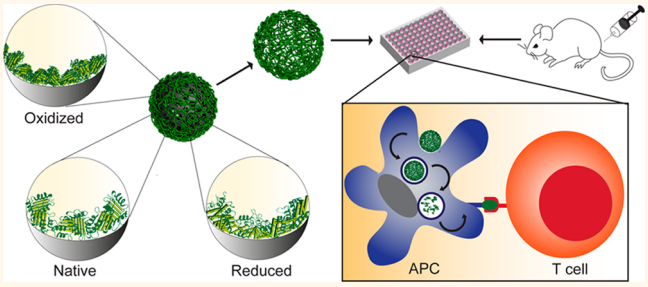

KEYWORDS: immunostimulation · biodegradation · vaccine · subunit antigen · phagocytosis · macrophage

The translation of subunit protein antigens into effective vaccines remains an important challenge in vaccine development due to the enhanced safety profiles of isolated proteins *versus* whole pathogens. Given the risks associated with whole pathogen-based vaccines, collaborative efforts in materials science and immunology have led to the development of a range of novel vaccine delivery formulations with improved characteristics.[1,2] Particle-based systems have shown particular efficacy due to their inherent immunogenicity.[3−9] Because antigens are typically highly sensitive to many chemical processes, changes in their structural and chemical properties can often occur during particle fabrication. Studies have shown that the efficacy of immune cell interactions is largely governed by an interplay of antigen properties, such as conformation,[10−12] structural stability,[13−15] the presence of disulfide bonds,[16,17] structural flexibility,[18] and the accessibility of protease cleavage sites,[19,20] all of which can be altered during chemical processes.

The use of disulfide bonds in material fabrication and surface functionalization strategies has become a widespread approach for engineering bioresponsive properties in particles for biomedical applications.[21,22] Redox-driven disulfide bond formation has been used to stabilize antigen carriers, such as virus-like particles[23] and polymer capsules,[24−27] and attach thiol-containing ligands to particle surfaces.[28,29] In these systems, exposure to oxidizing reagents (*e.g.*, oxidized glutathione, hydrogen

* Address correspondence to fcaruso@unimelb.edu.au.

Received for review July 24, 2014 and accepted February 15, 2015.

Published online February 25, 2015
10.1021/acsnano.5b00393

peroxide, diamide, chloramine-T) is employed to facilitate the formation of disulfide bonds within viral proteins,[23] within polymer carrier materials (post-antigen encapsulation),[24−26] or between cysteine thiols of proteins and ligands.[28,29] Due to the ubiquitous presence of thiols and disulfide bonds within many protein and peptide subunit antigens, it is likely that these processes result in a change in redox state. In addition, many thiol-reactive molecules (*e.g.*, tripeptide glutathione (GSH) and reactive oxygen species (ROS)) are present in various cellular environments. For example, GSH is abundant in the cytoplasm, ROS can be found in lysosomes and mitochondria, and many proteins containing thiols are expressed on cell surfaces. These thiols have been shown to play important roles in immune functions, such as T cell proliferation, and are tightly regulated during antigen presentation.[30] However, it remains unclear how the redox states of proteins in particle-based antigen formulations impact their interactions with cellular thiol-reactive molecules and the subsequent immune responses. As this information is key for rationally designing particle-based subunit antigen delivery systems, studies that address these questions are important in the field of vaccine delivery.

Well-defined and uniform particles can be used to evaluate specific parameters governing immune responses. Mesoporous silica (MS)-mediated assembly is a facile approach for fabricating particle systems with precise control over particle physicochemical properties, as well as cargo loading and release,[7,31−33] while ovalbumin (OVA) is a well-studied model antigen. To take advantage of these two aspects, herein we design a MS template-assembled pure OVA particle formulation stabilized through amide bonds and investigate the immunological influence of protein redox state. OVA contains four free thiols and one intrachain disulfide bond in its native structure.[34] By fabricating particles from native, reduced, and oxidized OVA, three types of particles with different structural properties were prepared (n-OVA, r-OVA, o-OVA particles, respectively), and the redox states were confirmed by measuring the degree of free thiol reactivity. We examined the interactions between the particles and innate immune cells by measuring phagocytosis, intracellular degradation, NFκB and AP-1 transcription factor activation, and cytokine secretion by a murine macrophage cell line, RAW 264.7 (RAW, ATCC TIB-71). Although RAW cells were able to bind and rapidly phagocytose all particles to a similar extent, resulting in activation of transcription factors and secretion of cytokines, the n-OVA and r-OVA particles were degraded more rapidly than o-OVA particles, suggesting different antigen processing occurred. Next, we evaluated the efficiency of immunogenic OVA epitope presentation by splenocyte antigen presenting cells (APCs) *ex vivo* and the capacity for priming T cells and generating immunoglobulin G (IgG) upon immunization *in vivo*. Our results show that slow intracellular degradability of oxidized OVA particles is correlated with inefficient OVA epitope presentation and immunogenicity *ex vivo* and *in vivo*. In contrast, particles fabricated from native and reduced OVA were found to elicit better T cell proliferative responses than free OVA and induce the highest levels of cytokine-producing CD4 T cells. In addition, both n-OVA and r-OVA particles were shown to stimulate the highest antibody titers after immunization compared with o-OVA particles. Combined, our results demonstrate that the different redox states of protein antigens lead to the generation of protein particles with variable physicochemical properties, including size, antigen loading, and protein density. These properties (in particular, particle density) have been shown to profoundly impact the antigen processing, giving rise to distinctively different immunogenicities. Given the likelihood that many currently used particle fabrication techniques result in changes to redox state and structure of protein antigens, this information is valuable knowledge for the development of effective and safe protein vaccines.

RESULTS AND DISCUSSION

Fabrication of Ovalbumin Particles with Different Redox States. Using MS templating and amide cross-linking, three types of pure ovalbumin particles with different redox states were fabricated (Figure 1a). Amine-functionalized MS templates (average diameter of 1 μm) were first loaded with native OVA (M_w 46 000) at pH 6, where OVA is negatively charged (isoelectric point = 4.6). Reduced and oxidized OVA particles were generated by treating the OVA-loaded MS particles with a reducing agent (DTT) or an oxidizing agent (chloramine-T). Then, particles containing either native, reduced, or oxidized OVA were stabilized through amide bond cross-linking using 4-(4,6-dimethothy-1,3,5-triazin-2-yl)-4-methylmorpholinium chloride, a nontoxic coupling reagent that can be removed from the postreaction mixture.[35] Stable, freestanding, single-component OVA particles were obtained after template removal. TEM images (Figure 1b−d) were used to measure particle size (Table 1) and visualize particle morphology. Images revealed distinct size and morphological differences between the particles as a result of oxidation and reduction of the protein. Oxidation resulted in smaller particles of about 460 ± 70 nm, approximately half the size of n-OVA and r-OVA particles, which were 930 ± 160 and 810 ± 140 nm, respectively. Further, the o-OVA particles showed a high contrast compared with n-OVA and r-OVA particles in TEM images, suggesting a high protein density. Oxidation of proteins leads to alterations in protein structure *via* the formation of new disulfide bonds.[36] The addition of new disulfide bonds

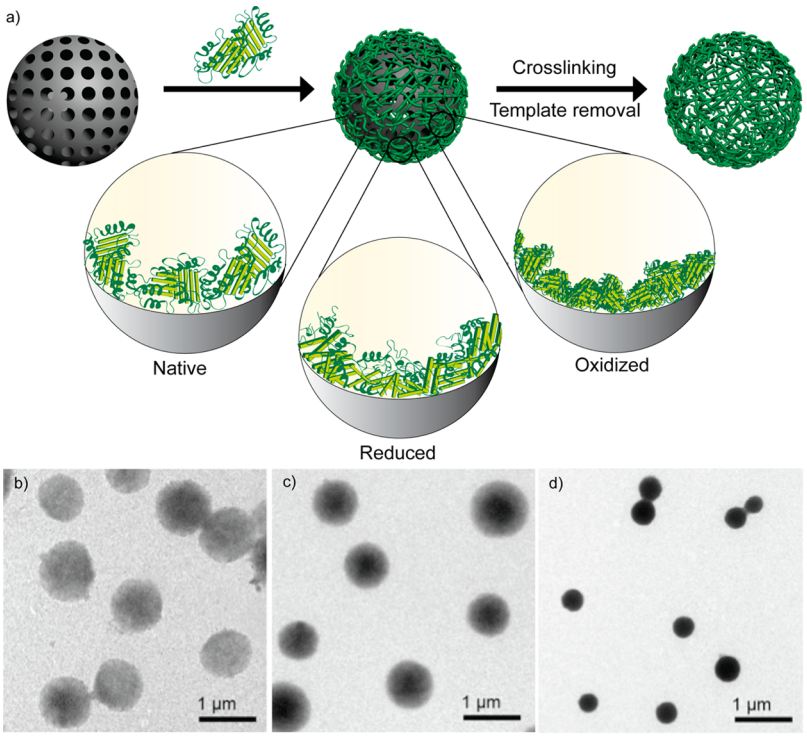

Figure 1. (a) Schematic representation of the fabrication of n-OVA, r-OVA, and o-OVA particles where loaded ovalbumin is native, oxidized, or reduced within MS templates prior to amide bond cross-linking and template removal. TEM images of n-OVA (b), r-OVA (c), and o-OVA particles (d).

TABLE 1. Characterization of OVA Particles: Size (from TEM), Mass of OVA per Particle, Density of OVA, and Zeta Potentials of n-OVA, r-OVA, and o-OVA particles

	size (nm)	OVA/particle (ng) ($\times 10^{-4}$)	OVA density (ng/nm^3) ($\times 10^{-13}$)	zeta potential (mV)	zeta potential 10% FBS (mV)
n-OVA	930 ± 160	1.2 ± 0.1	2.9 ± 0.9	−20 ± 8	−17 ± 4
r-OVA	810 ± 140	1.4 ± 0.1	5.1 ± 1.6	−21 ± 4	−17 ± 4
o-OVA	460 ± 70	1.8 ± 0.2	36.1 ± 11.0	−24 ± 4	−17 ± 4

has been shown to enhance the structural stability of free proteins.[15] Within the particle, the formation of new disulfide bonds also seems to enhance the structural stability of the protein network, which explains the shrinkage of the particles upon template removal. The r-OVA particles appeared to be slightly smaller with a higher contrast and more uniform density compared with n-OVA particles. Reduction of OVA with DTT has been shown to successfully cleave the native intrachain disulfide formed between Cys73 and Cys120, exposing domains that were previously hidden in the native conformation.[37] We assume that this conformational alteration leads to changes in the intra- and interprotein attractive forces (*e.g.*, covalent, electrostatic, van der Waals), resulting in size and morphological changes in the r-OVA particles.

On the basis of the total number, mass, and size of the particles, the average OVA loading capacity and OVA density were calculated for each particle (Table 1). Results showed similar loading capacities across all particles, leading to variations in OVA density due to particle size, confirming that TEM data accurately represents protein density. While r-OVA and n-OVA particles had a similar density, o-OVA particles had a higher average density that was more than 12- and 7-fold higher than n-OVA and r-OVA particles, respectively. These results suggest that variations in protein redox states influence the structure of the protein network even if the same cross-linking strategy is used (*i.e.*, amide cross-linking).

To confirm that the exposure of the OVA proteins in the MS templates to oxidizing and reducing conditions led to alteration of the native free thiols and disulfide bonds, free thiol groups in each particle were qualitatively determined by measuring their reactivity toward a maleimide-conjugated fluorescent dye (Alexa Fluor 488-maleimide) using flow cytometry. To verify the specificity of the reaction, n-OVA and r-OVA particles were also pretreated with excess 2,2′-dinitro-5, 5′-dithiobenzoic acid (DTNB, Ellman's reagent) for 6 h to block the free thiols and inhibit their reactivity toward the maleimide. DTNB-treated and untreated particles were incubated with excess fluorescent label and washed extensively, and the mean fluorescence

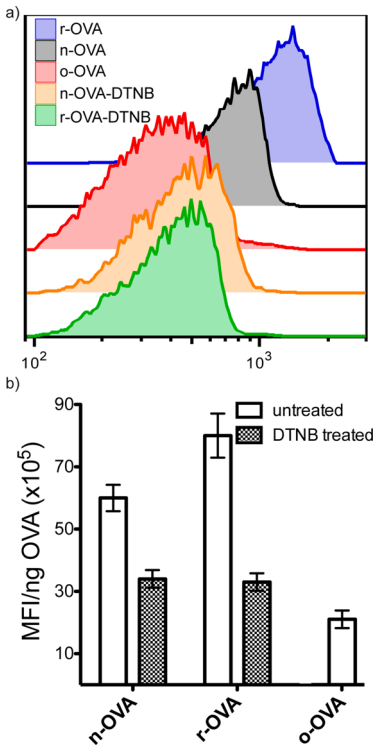

Figure 2. (a) Fluorescence intensity histograms of r-OVA (blue), n-OVA (gray), and o-OVA (red) particles labeled with Alexa Fluor 488 maleimide reactive dye. As a control, DTNB was used to block thiols on n-OVA (orange) and r-OVA (green) particles before labeling. (b) MFI/ng of OVA based on the mass of OVA per particle of n-OVA, r-OVA, and o-OVA particles (white bars) and n-OVA and r-OVA pretreated with DTNB (gray bars).

intensity (MFI) was measured using flow cytometry (Figure 2a). Results showed that the MFI of o-OVA and r-OVA particles was shifted to lower and higher values compared with n-OVA particles, respectively. Additionally, pretreatment with DTNB resulted in MFI values similar to those observed for o-OVA particles, confirming the specificity of the thiol−maleimide reaction. To correct for differences in protein content per particle, MFI per ng of OVA was also calculated based on OVA loading capacity (Figure 2b). As expected, the r-OVA particles resulted in the highest MFI/ng, followed by n-OVA and o-OVA particles, respectively. These data confirm that treatment of the OVA with reducing and oxidizing agents alters the native thiols and disulfide bonds within OVA proteins, leading to particles with different redox states. Additionally, the zeta potentials of the particles were not altered as a result of changing the protein redox state: they were determined to be approximately −20 mV in 10 mM Dulbecco's phosphate buffered saline (DPBS) for all three particles (Table 1). Because cell experiments *in vitro* and *ex vivo* were conducted in Dulbecco's modified Eagle's medium (DMEM) containing 10% fetal bovine serum (FBS), surface adsorption of proteins can influence the zeta potentials of the particles. To measure this effect, particles were incubated in complete cell culture medium for 1 h at 37 °C, centrifuged, and redispersed in 10 mM DPBS for zeta potential measurements. Results showed a cumulative increase in zeta potential, where all particles had a zeta potential of −17 mV.

Adherence, Phagocytosis, and Degradation of OVA Particles by Macrophages. A mouse macrophage cell line (*i.e.*, RAW) was employed as a model APC to investigate the cellular association (including cell surface bound and internalized), intracellular degradation, and immunogenicity of the OVA particles. Macrophages are phagocytic cells of the innate immune system that have specifically evolved to internalize particulate material through a specialized form of endocytosis called phagocytosis.[38] Phagocytosis is a necessary process for eliciting robust immune responses to particulate material whereby antigen processing and presentation pathways are accessed *via* the phagosome,[39] which has a characteristically low pH of approximately 5.[40] Hence, pH-sensitive fluorophores have been employed to evaluate the acidification of particle-containing phagosomes.[41] Using particles labeled with both pH-independent and pH-dependent fluorophores, the difference in associated (both surface bound and internalized) and phagocytosed particles could be determined by detecting the signal from the respective labels using flow cytometry and fluorescence deconvolution microscopy. The fluorescence of Alexa Fluor 633 (AF633) is insensitive to a wide pH range, including physiological and phagosomal pH, making it well suited for detecting both adhered and internalized particles. pHrodo-Red (Life Sciences, Pty Ltd., NSW, Australia) is a pH-sensitive fluorochrome that has been used to examine phagocytosis.[42] The fluorescence of pHrodo-Red significantly increases in acidic conditions, such as those found within the macrophage phagosome, allowing the determination of phagocytosed particles.

The percentage of cells with either associated (*i.e.*, positive AF633 signal) or phagocytosed (*i.e.*, positive pHrodo-Red signal) particles was measured after incubating RAW cells with particles at 37 °C and 5% CO_2 for 1, 3, 6, and 24 h time intervals. At 1, 3, and 6 h, the total association and phagocytosis of o-OVA particles by macrophages was slightly greater compared to the n-OVA or r-OVA particles (Figure 3a). At 24 h, however, the percentage of macrophages with both associated or phagocytosed particles was not significantly different, reaching over 90% of particle-associated cells. Previous reports have indicated a close relationship between cellular uptake and the physicochemical parameters of particles, including size, morphology, and charge.[43] Given that the zeta potentials are similar for the particles examined (Table 1), the variation observed may reflect size and morphological differences. Consistent with the literature, the results indicate a correlation between particle structural properties and cellular uptake, where smaller, denser

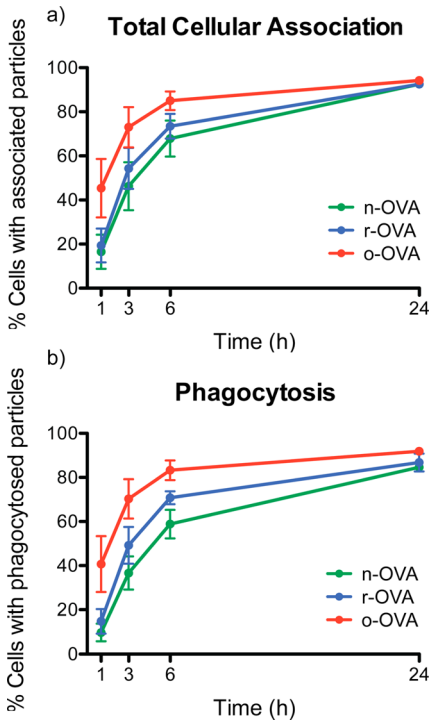

Figure 3. Percentage of RAW cells with (a) associated or (b) phagocytosed n-OVA (green), r-OVA (blue), and o-OVA (red) particles measured by flow cytometry. Cells were incubated with particles at a particle-to-cell ratio of 100:1 at 37 °C, 5% CO_2. Data are the mean ± standard deviation of three independent experiments.

particles, such as the o-OVA particles, can interact with APCs more efficiently.[44,45] For all three types of particles, flow cytometry results showed marginal differences between cells with associated and phagocytosed particles, suggesting that rapid internalization occurs following initial cell membrane binding. Deconvolution microscopy images acquired after 3 h of incubation (Figure 4) further confirmed this finding, where most of the particles yield both AF633 (Figure 4a–c) and pHrodo-Red signals (Figure 4d–f).

Intracellular degradation of the OVA particles was determined by visualization of RAW cells with internalized particles using fluorescence deconvolution microscopy. In this experiment, fluorescently labeled particles were incubated with RAW cells for 1, 3, and 6 h time intervals, and unassociated particles were removed by extensive washing with DPBS prior to imaging using deconvolution microscopy. Illustrated by the first appearance of these fluorescent particle fragments, n-OVA and r-OVA particles showed initial degradation at 3 h incubation and an increased occurrence of these fragments after 6 h (Figure 5a–f). The o-OVA particles, however, were degraded much slower, with the generation of only a few intracellular fragments, even after 6 h (Figure 5g–i). To quantitatively compare the morphological changes of the internalized particles due to degradation, the fluorescent

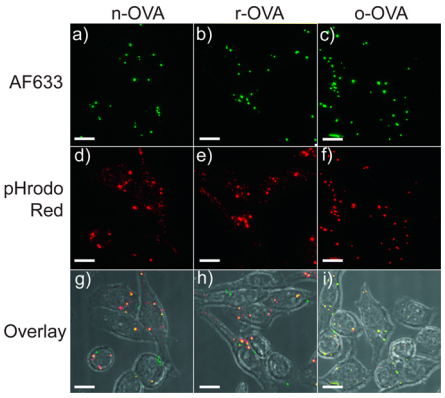

Figure 4. Phagocytosis of n-OVA, r-OVA, and o-OVA particles after 3 h of incubation at 37 °C, 5% CO_2, visualized by live deconvolution microscopy. The cellular association of the particles is shown by AF633 signal (a–c, green), and phagocytosed particles are shown by pHrodo Red signal (d–f, red). (g–i) Bright-field and fluorescence images are overlaid. All images are shown as maximum intensity projections. All scale bars = 10 μm.

particle volume was analyzed using Imaris 6.3.1 software (Bitplane) (Figure 5j–l). First, based on fluorescent intensity, particles with variable sizes were identified using a built-in particle detection function. A reference diameter of 1 μm was set to normalize the change of particle volume at different time intervals. The distribution of the normalized particle volume was calculated and compared (Figure 5j–l). The analysis shows that the volume of n-OVA and r-OVA particles decreased rapidly after 3 h of incubation, suggesting that they are degraded at a similar rate. In contrast, larger volumes of o-OVA particles remained after 6 h of incubation. These results indicate that the obtained protein particles fabricated from native and reduced OVA are quickly degraded in intracellular compartments. However, exposure of the OVA to oxidizing conditions during particle fabrication significantly inhibited the susceptibility of particles to intracellular degradation.

To further delineate the role of protein density and disulfide bonding in intracellular degradation, o-OVA particles were exposed to DTT for 1 h at 37 °C to reduce the disulfide bonds. To verify the reduction of disulfide bonds, particles were labeled with a maleimide-conjugated fluorophore and the MFI was measured (Figure S1). A similar experiment comparing the intracellular degradation of o-OVA and reduced o-OVA particles in RAW cells showed no apparent differences at the time points examined (Figure S2).

Intracellular degradation of proteins is highly dependent on the accessibility of enzymatic cleavage sites. For enzymes to gain access to various sites within the protein, the 3D structure must be unfolded.[46] Structural changes in the particles induced by oxidation and reduction were likely the result of alterations in covalent and noncovalent interactions. Oxidation increases the structural stability of the protein particle

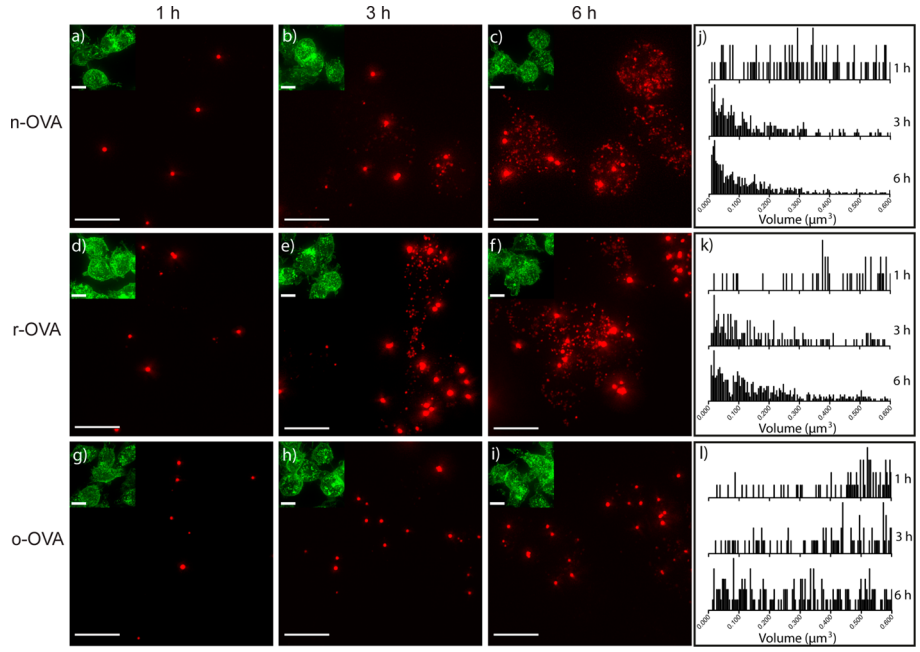

Figure 5. Intracellular degradation of (a–c) n-OVA, (d–f) r-OVA, and (g–i) o-OVA visualized by fluorescence deconvolution microscopy after incubation for (a, d, g) 1 h, (b, e, h) 3 h, and (c, f, i) 6 h at a particle to cell ratio of 100:1 at 37 °C, 5% CO_2. Maximum intensity projection images show the cell membrane (stained with Alexa Fluor 488-wheat germ agglutinin, green, insets) and Alexa Fluor 633-labeled particles (red). Particle volumes were analyzed in Imaris 6.3.1 software using a reference diameter of 1 μm for (j) n-OVA, (k) r-OVA, and (l) o-OVA particles at 1, 3, and 6 h time intervals. All scale bars = 10 μm.

matrix, evidenced by the increase of disulfide bonds and high OVA density. Structural constraints induced by disulfide bonds,[15,47,48] chemical cross-links,[16] and noncovalent interactions[13] have been shown to reduce the susceptibility of free soluble proteins to proteolytic digestion, which is in good agreement with the current findings. In the particle formulation, oxidation and reduction changed the disulfide bonding within the particles, which caused differences in their physical properties (*i.e.*, protein density). Reduction of disulfide bonds facilitates protein unfolding and has been shown to increase the susceptibility of free cysteine-containing proteins to enzymatic degradation.[47,48] Particle density, however, determines enzymatic permeability throughout the protein matrix. Our data have shown that n-OVA and r-OVA particles with similar particle density but a different number of thiols exhibited similar intracellular degradation. Similarly, the reduced o-OVA particles showed a consistently prolonged intracellular degradation profile compared with o-OVA. Taken together, these results suggest that OVA particle density plays a major role in controlling the intracellular degradation kinetics.

APC Activation and Cytokine Secretion. In addition to antigen presentation, APCs are responsible for activating and shaping adaptive immune responses by providing contextual cues such as secreted cytokines. This occurs as a result of antigen binding to APC receptors on the cell surface and within intracellular compartments. Activation of the transcription factors can occur in response to receptor binding and is necessary for inducing cytokine secretion. NFκB and AP-1 transcription factor activation was measured by incubation of the particles with RAW-Blue cells, a reporter cell line that expresses all TLRs (except TLR5), RIG-I, MDA-5, NOD1, and NOD2. RAW-Blue cells are derived from RAW macrophages that express a secreted embryonic alkaline phosphatase (SEAP) gene. Recognition of receptor agonists activates NFκB and AP-1, which induces SEAP with quantitative absorbance levels. The n-OVA, r-OVA, and o-OVA particles showed significantly stronger activation compared with control cells at concentrations above 10 particles per cell, indicating dose-responsive, particle-induced activation of NFκB and AP-1 (Figure 6a).

The activation of transcription factors is a crucial step in the secretion of cytokines by APCs necessary for expressing an immune context and activating other immune cells. Using a cytokine bead array assay (Bio-Plex assay), the concentrations of various cytokines were measured following incubation of particles with RAW cells for 24 h (Figure 6b–f). In agreement with transcription factor activation, a dose-responsive secretion of IL-1β, IL-9, IL-12p70, IL-10, and IL-13 was observed for the particles. The results indicate that despite slight differences in phagocytosis and significant differences in intracellular degradation, all of the particles induce similar levels of macrophage activation and cytokine response.

T Cell Activation. The immunogenicity of the particles was investigated through a series of assays that measure the induction of OVA-specific T cell responses.

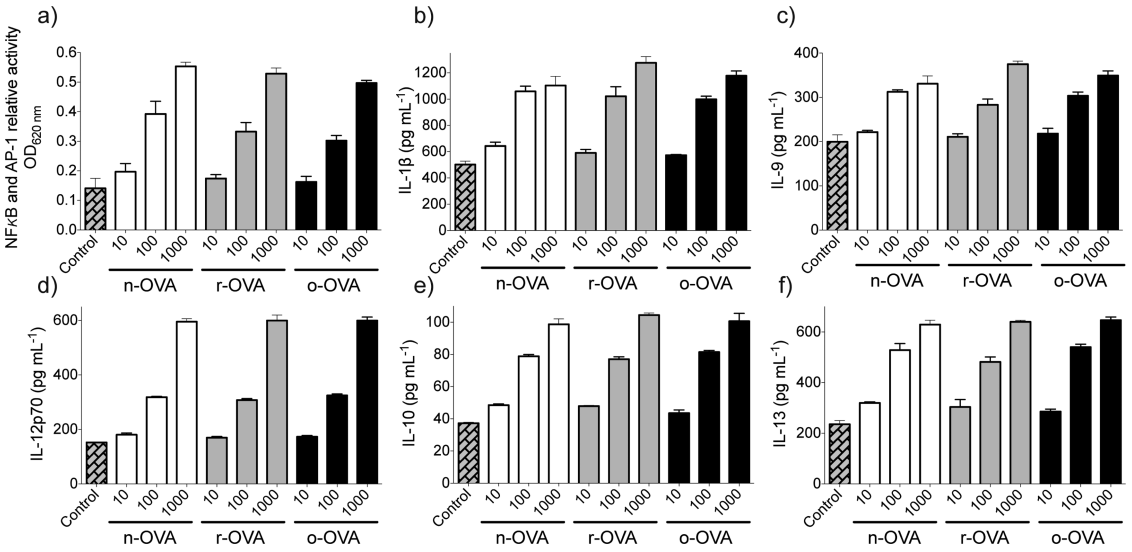

Figure 6. (a) NFκB and AP-1 transcription factor activation in RAW-Blue cells measured by optical density at 620 nm of SEAP secretion. Concentration of (b) IL-1β, (c) IL-9, (d) IL-12p70, (e) IL-10, and (f) IL-13 cytokine secretion by RAW cells induced by n-OVA, r-OVA, and o-OVA particles at 10:1, 100:1, and 1000:1 particle to cell ratios at 37 °C, 5% CO_2.

The presentation of immunogenic OVA epitopes was investigated by stimulating OVA-primed T cells with APCs and particles *ex vivo* and measuring their proliferation and cytokine secretion. Mice (C57BL/6) were initially immunized with free OVA emulsified with incomplete Freund's adjuvant (IFA), a strong adjuvant mixture that results in proliferation of OVA-specific T cells. One week following immunization, the draining lymph nodes were harvested and OVA-primed T cells were isolated using anti-CD90.2 magnetic bead sorting. Syngeneic APCs (mytomycin C-treated splenocytes) from naïve mice were preincubated for 1 h prior to addition of OVA-primed T cells with serial dilutions of either free soluble OVA, n-OVA, r-OVA, or o-OVA particles at equivalent total protein levels. The extent of antigen-specific T cell proliferation was then determined following 4 days of incubation by the incorporation of ^{3}H-thymidine. In comparison to the equivalent free soluble OVA, a significantly enhanced T cell proliferative response was found at eight different antigen doses for r-OVA particles, four different antigen doses for n-OVA particles, and two doses for o-OVA particles, respectively (Figure 7a, Table S1 for statistical analysis, two-way ANOVA analysis). This suggests an increase in potency of immune responses induced by particulate antigen carriers compared with free soluble antigen, which is in agreement with other studies.[6,25,49,50] It is also noted that r-OVA showed significantly enhanced T cell proliferation compared to n-OVA or o-OVA particles at a certain dose, although for most of the doses no significant differences were found between the three types of particles (Figure 7a, Table S1).

To further investigate the functions of the stimulated T cells, an ELISPOT assay was used to determine T cell differentiation (T helper 1 (Th1) *versus* T helper 2 (Th2)) by measuring the number of T cells producing either IFN-γ or IL-4 cytokines, respectively. r-OVA particles induced significantly more IL-4-secreting T cells than n-OVA ($p < 0.05$) and o-OVA ($p < 0.001$) particles. Similar trends were also observed in IFN-γ-producing T cells (Figure 7b, Table S2 for statistical analysis, one-way ANOVA analysis). Overall, the results indicated a Th1-polarized proinflammatory response where all OVA particles stimulated a higher number of IFN-γ-producing T cells compared with IL-4 (Figure 7b). Studies have indicated that processes leading to antigen presentation occur quickly after internalization.[51] Rapid degradation kinetics of both free proteins[15,17] and antigen particle carriers[52] is favorable for efficient antigen presentation. In good agreement, our data also demonstrate a correlation between intracellular particle degradation and OVA-specific immunogenicity. Slow intracellular degradation of o-OVA particles results in a significant reduction of OVA epitope presentation by APCs in comparison to r-OVA and n-OVA particles. Moreover, the difference between r-OVA and n-OVA suggests that a reduced redox state can further facilitate the OVA epitope presentation to T cells, although their intracellular degradation based on the morphological changes *in vitro* did not exhibit significant variations.

The immunogenicity *in vivo* was investigated by measuring OVA-specific T cell responses following immunization with the particles. The efficiency of OVA-specific T cell priming *in vivo* was determined by measuring T cell differentiation in response to soluble OVA stimulation *ex vivo* using an ELISPOT assay described above. T cells from mice immunized with a 1:1 oil-in-water emulsion of PBS and IFA were used as negative controls (Figure S3), which as expected, failed to exhibit any OVA-specific T cell response. Stimulation of T cells obtained from mice immunized with r-OVA particles resulted in significantly more

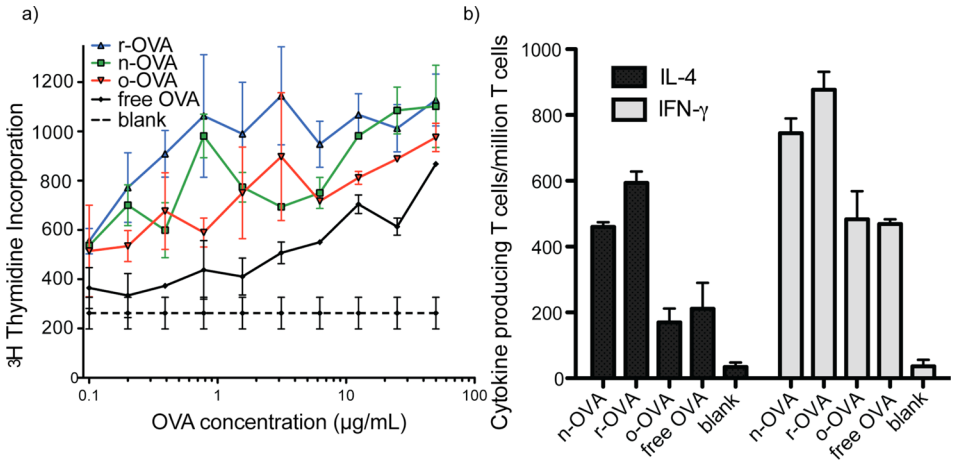

Figure 7. (a) T cell proliferation of OVA-primed CD4 T cells stimulated with naïve splenocyte APCs and o-OVA (red), n-OVA (green), r-OVA (red), and free OVA (black) at 37 °C, 5% CO_2 *ex vivo* for 4 days at various concentrations measured by the cellular incorporation of ^{3}H-thymidine. T cell proliferation in the absence of antigen stimulation (*i.e.*, blank) is shown as a black dotted line. (b) Number of IL-4- (black bars) and IFN-γ-producing (gray bars) T cells per million T cells when stimulated with splenocyte APCs and 2.5 μg of either OVA particles (n-OVA, r-OVA, o-OVA) or free soluble OVA at 37 °C, 5% CO_2 *ex vivo* for 3 days measured using an ELISPOT assay. Statistical analyses are shown in Tables S1 and S2.

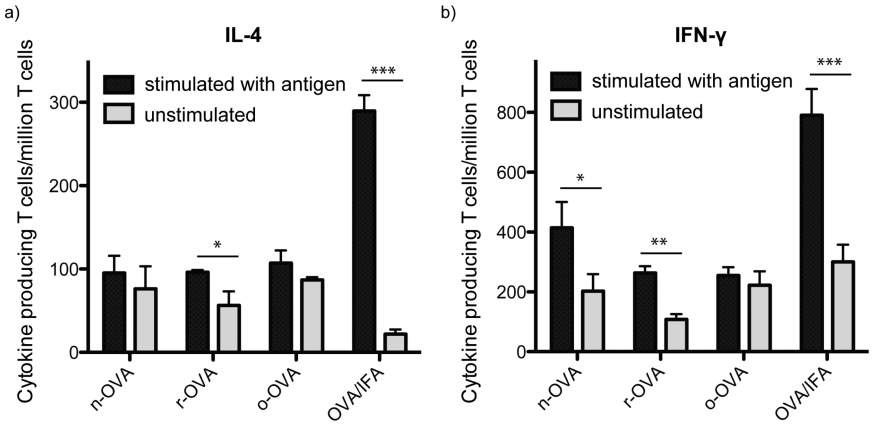

Figure 8. Mice were subcutaneously immunized with particles or an emulsion of OVA and IFA (positive control) and subsequently stimulated by incubation with naïve splenocyte APCs at 37 °C, 5% CO_2 *ex vivo* for 3 days, and the production of IL-4 (a) and IFN-γ (b) by T cells was measured in the presence (black bars) and absence (gray bars) of free soluble OVA using an ELISPOT assay. *$p < 0.05$; **$p < 0.01$; ***$p < 0.001$, *t*-test.

IL-4- and IFN-γ-producing T cells compared with the blank samples (*i.e.*, unstimulated). n-OVA particle-primed T cells also showed significant increases in IFN-γ-secreting T cells in the presence of free OVA. This suggests that r-OVA and n-OVA particles are capable of priming T cells to specifically respond to ovalbumin when injected *in vivo*. However, T cells from o-OVA-immunized mice did not respond to antigen stimulation, indicating that the particles did not efficiently prime OVA-specific T cells *in vivo*. Given the correlation between the current results, intracellular degradation (Figure 5), and OVA epitope presentation (Figure 7), it is likely that antigen-specific T cell priming *in vivo* is directly affected by the efficiency of intracellular degradation and OVA epitope presentation by APCs.

B Cell Activation. Protective immunity is highly dependent on antibody secretion by plasma B cells, and the measurement of serum antibody titers remains the gold standard for quantifying vaccine performance in clinical trials. B cell immune responses were evaluated using an enzyme-linked immunosorbent assay (ELISA) to measure the total OVA-specific IgG present in the serum following a primary and secondary immunization. In the experiment, mice were given a primary intraperitoneal immunization of n-OVA, r-OVA, and o-OVA particles and a booster subcutaneous immunization 2 weeks later. Naïve mice and mice immunized with OVA and IFA were used as negative and positive controls, respectively. The results showed that the sera obtained from mice immunized with n-OVA and r-OVA particles contained statistically similar levels of IgG that were significantly higher than sera from mice immunized with o-OVA particles ($p < 0.001$) (Table S3 for statistical analysis, one-way ANOVA analysis). In fact, the sera from mice immunized with o-OVA particles contained no detectable OVA-specific IgG similar to

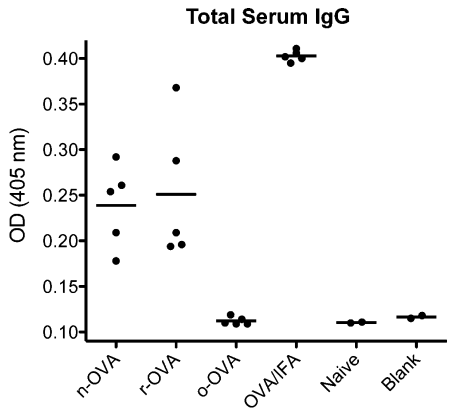

Figure 9. Total OVA-specific IgG in the sera of n-OVA-, r-OVA-, o-OVA-, and OVA/IFA-immunized and naïve mice. Sera were diluted 100 times, and the total IgG was measured using an ELISA assay. Antibody titers are expressed as the absorbance of the solution at 405 nm. Each group contains data from the sera of five different mice. Statistical analysis is shown in Table S3.

naïve and blank control samples. Activation and antibody secretion by B cells is typically dependent on costimulation from activated T helper cells. The negligible level of serum IgG stimulated by o-OVA particles is consistent with the poor T cell activation *ex vivo* (Figure 7) and *in vivo* (Figure 8).

CONCLUSIONS

The current study presents an analysis of the physicochemical and immunological consequences of oxidation and reduction of a protein antigen (*i.e.*, OVA) formulated within a mesoporous silica-templated, amide cross-linked particle system. Our data show that redox modifications affect both the physicochemical properties (*i.e.*, size, morphology, density, redox state) and the immunogenic performance of the particles. Our results also show that despite the redox-induced physicochemical differences among the particles, innate immunogenicity is not largely affected (*i.e.*, phagocytosis, NFκB and AP-1 transcription factor activation, cytokine secretion). However, oxidation is shown to inhibit the rate of intracellular degradation of the particles compared with those fabricated from native and reduced protein, most likely due to increased protein density. The slow intracellular degradation of the oxidized protein particles is correlated with inefficient epitope presentation and insignificant levels of antibody secretion *in vivo*, therefore suggesting the direct impact of antigen degradability on adaptive immune responses. Taken together, the current study demonstrates how the redox state of protein antigens in particle-based formulations can affect antigen intracellular processing, which is a prerequisite for antigen presentation and subsequent adaptive immune responses. Given that protein antigens are typically highly susceptibility to structural alteration during chemical processing (*e.g.*, reduction and oxidation), our understanding of these changes and their associated immunological impacts is important for optimizing particle formulations for protein antigen delivery.

METHODS

Materials. Albumin from chicken egg white (OVA), (3-aminopropyl)triethoxysilane (APTES), 2-(*N*-morpholino)ethanesulfonic acid hydrate (MES), poly(acrylic acid) (PAA), cetyltrimethylammonium bromide (CTAB), tetraethyl orthosilicate (TEOS), 3-(*N*-morpholino)propanesulfonic acid (MOPS), *N*-chloro-*p*-toluenesulfonamide sodium salt (chloramine-T), 5,5′-dithiobis-(2-nitrobenzoic acid) (DTNB), hydrofluoric acid (HF), dithiothreitol (DTT), 4-(4,6-dimethoxy-1,3,5-triazin-2-yl)-4-methylmorpholinium chloride (DMTMM), 0.25% trypsin-EDTA solution, red blood cell lysing buffer, mytomycin-C, incomplete Freund's adjuvant (IFA), goat anti-mouse, horseradish peroxidase swine anti-goat, and 2,2′-azinobis(3-ethylbenzothiazoline-6-sulfonic acid) (ABTS) were purchased from Sigma-Aldrich and used as received. Paraformaldehyde (4%) was purchased from Electron Microscopy Sciences, USA. Alexa Fluor 633 maleimide and succinimidyl ester and pHrodo red succinimidyl ester reactive dyes, Dulbecco's modified Eagle's medium containing L-glutamine and glucose (DMEM), heat-inactivated fetal bovine serum (HI-FBS), Dulbecco's phosphate-buffered saline, and Alexa Fluor 488 wheat germ agglutinin were purchased from Life Technologies. Quanti-Blue and Normocin were purchased from InvivoGen. 3H-Thymidine was purchased from GE Healthcare Life Sciences. Ultrapure water with resistance greater than 18 MΩ cm was obtained from an inline Millipore RiOs/Origin system (Millipore Corporation, USA).

Preparation and Amine-Functionalization of MS Templates. MS particles were synthesized according to a modified literature method.[53] Briefly, 1.1 g of CTAB was completely dissolved in 50 mL of water with stirring. Subsequently, 4.3 g of PAA solution was added with vigorous stirring at room temperature (RT) (25 °C) until a clear solution was obtained. Next, 3.5 mL of ammonium hydroxide solution was added to the above solution with vigorous stirring, resulting in a milky suspension. After stirring for 20 min, 4.46 mL of TEOS was added to the above solution. After further stirring for 15 min, the mixture was transferred into a Teflon-sealed autoclave, which was left at 100 °C for 48 h. The as-synthesized MS particles were washed with Milli-Q water and ethanol three times and finally dried at 80 °C overnight. The organic templates were removed by calcination at 550 °C for 6 h. A 30 mg amount of the synthesized MS particles was dispersed in 900 mL of 70% (v/v) ethanol, followed by incubation with 50 μL of ammonia solution and 30 μL of APTES overnight. The modified particles were washed with ethanol and Milli-Q water three times.

Preparation of Particles from Native, Oxidized, and Reduced Ovalbumin. APTES-modified MS particles (2 mg mL^{-1}) were dispersed in 2 mg mL^{-1} native OVA solution in MES buffer (50 mM, pH 6). The particle dispersion was allowed to incubate for 4 h at RT with constant agitation to allow OVA infiltration *via* electrostatic surface adsorption into the MS network. Following incubation, excess OVA was removed by centrifugation, and particles were washed with MES buffer. Oxidation of OVA was achieved by dispersing 2 mg mL^{-1} MS particles with loaded OVA (described above) in MES buffer (50 mM, pH 6) containing 2 mg mL^{-1} chloramine-T for 5 min. Reduction of OVA was achieved by dispersing 100 mg mL^{-1} MS particles with loaded OVA in MOPS buffer (20 mM, pH 8) containing 77 mg mL^{-1} DTT for 30 min at 37 °C with constant agitation. Following oxidation and reduction, the particles were washed with MES buffer. Native, reduced, or oxidized OVA was cross-linked within the MS particles by dispersing 5 mg mL^{-1} MS particles in MES buffer

(50 mM, pH 6) containing 10 mg mL^{-1} DMTMM and allowed to incubate overnight (~16 h) at room temperature (RT) with constant agitation. MS templates were dissolved with 2 M HF/8 M NH_4F solution (pH ~5). *Caution! HF is highly toxic. Extreme care should be taken when handling HF solution, and only small quantities should be prepared*. The resulting OVA particles were washed with Milli-Q water.

Measuring Particle Size and Quantification of OVA per Particle. Particle size was measured using TEM images of at least 120 different particles. n-OVA, r-OVA, and o-OVA particles were counted using an Apogee A50-micro flow cytometer using small- and large-angle scattering to determine the number of particles per volume. Aliquots (>1 mg) were weighed on a standard analytical mass balance to determine the mass of OVA per volume. Mass of OVA per particle was calculated based on the total number and mass of particles.

Determination of Free Thiol Content. The free thiol content within the particles was qualitatively determined by dispersing 2 mg mL^{-1} OVA particles in DPBS buffer containing excess Alexa Fluor 488 maleimide and allowed to incubate for 6 h at RT with constant agitation. Excess label was removed by centrifugation, and particles were washed with Milli-Q water. The MFI of the particles was measured using an Apogee A50 micro flow cytometer. The MFI to protein weight ratio was calculated based on the OVA loading capacity. Control particles were first dispersed in 2 mg mL^{-1} DTNB and allowed to incubate for 6 h at RT with constant agitation. Particles were washed with DPBS *via* centrifugation prior to labeling.

Zeta Potential Measurements. Zeta potentials were measured using a Malvern Zetasizer Nano ZS (Worcestershire, UK) at 25 °C. Particles (1×10^7) were dispersed in 10 mM DPBS. To assess zeta potential changes as a result of protein adsorption in cell culture media, particles were incubated in cell culture media for 1 h at 37 °C, centrifuged, and redispersed in 10 mM DPBS prior to the measurement.

Dual Fluorescent Labeling. Particles were labeled with equal concentrations of both Alexa Fluor 633 succimidyl ester and pHrodo Red succimidyl ester in DPBS buffer containing 0.1 M $NaHCO_3$ for 2 h at RT with constant agitation. Excess label was removed by centrifugation, and particles were washed with Milli-Q water.

Cell Culture. RAW 264.7 cells were maintained in DMEM with the addition of 10% (v/v) HI-FBS at 37 °C in a 5% CO_2 humidified atmosphere.

Cellular Association and Phagocytosis of Particles by Flow Cytometry. The cellular association and phagocytosis were quantified as described previously.[54] RAW cells were plated at a concentration of 10^5 cells in 500 μL of growth media in 24-well plates and allowed to incubate overnight (~16 h) at 37 °C, 5% CO_2. Dual-labeled (AF633 and pHrodo red) particles (10^7) were then added and allowed to further incubate for varying time intervals. After incubation, unassociated particles were removed from adherent cells by gently washing with DPBS. Cells were removed from plates by treatment with 0.25% trypsin/EDTA solution (200 μL/well) for 5 min at 37 °C, 5% CO_2. Complete DMEM (300 μL/well) was then added to inhibit trypsin activity. Cell suspensions were collected and centrifuged at 300*g* for 5 min. The cell pellet was resuspended in DPBS and analyzed by flow cytometry (Apogee A50 micro flow cytometer). At least 10^4 cells were analyzed for each sample. The data are presented as a percentage of cells associated with particles.

Fluorescence Deconvolution Microscopy for Cellular Uptake and Intracellular Degradation. RAW cells were plated at a concentration of 6.4×10^4 cells in 250 μL of growth media in an eight-well Lab-Tek II Chambered #1.5 coverglass system (Thermo Fisher Scientific) and allowed to incubate overnight (~16 h) at 37 °C, 5% CO_2. Dual-labeled (AF633 and pHrodo red) particles (6.4×10^6) were then added and allowed to incubate for varying time intervals. Excess particles were removed by gently washing cells with DPBS. For intracellular degradation experiments, the cells were fixed with 4% paraformaldehyde for 20 min at RT. The cell membrane was stained with Alexa Fluor 488-wheat germ agglutinin (5 μg mL^{-1}) in DPBS at RT for 10 min. Optical sections of cell images were collected using a fluorescence deconvolution microscope (Delta Vision, Applied Precision). Images were processed with Imaris 6.3.1 software (Bitplane), and fluorescence and bright-field images were presented in maximum intensity projection.

RAW-Blue NFκB and AP-1 Activation Assay. RAW-Blue cells (InvivoGen, CA, USA) were plated at a concentration of 10^5 cells in 200 μL of DMEM containing 10% HI FCS, 2 mM L-glutamine, and 100 μg mL^{-1} Normocin, in a V-bottom 96-well plate. Particle to cell ratios of 10:1, 100:1, and 1000:1 were added to the cells and allowed to incubate for 24 h at 37 °C, 5% CO_2. A 50 μL portion of supernatant was taken from the cultures, and 150 μL of Quanti-Blue was added and allowed to incubate for 2 h. Optical density was measured at 620 nm to quantify SEAP levels.

Bio-Plex Cytokine Secretion Assay. RAW cells were plated at a concentration of 10^5 cells in 200 μL of complete DMEM in a flat-bottom 96-well plate. Particle to cell ratios of 10:1, 100:1, and 1000:1 were added to cells and allowed to incubate for 24 h at 37 °C, 5% CO_2. Supernatant was removed and spun at 8000*g* to remove particulate matter before being stored at −30 °C. Cytokine levels in the supernatants were measured using a Bio-Plex Pro mouse cytokine standard 23-plex, group 1 kit (Bio-Rad, NSW, Australia) on a Bio-Plex 200 System (Bio-Rad) as previously described[55] and using the manufacturer's instructions.

Mice. C57BL/6 mice were obtained from the Walter and Eliza Hall Institute (WEHI) animal facility and were housed in specific pathogen-free conditions at the Biological Research Facility in the Royal Dental Hospital of Melbourne. Animal experimentation was approved by the University of Melbourne Animal Ethics Committee.

APC Preparation. Spleens were taken from naïve mice, and single-cell suspensions were prepared using a gentleMACS. Red blood cells were lysed using red blood cell lysing buffer. Cells were inactivated using mytomycin-C.

Immunization and T Cell Preparation. Mice were immunized subcutaneously with either 1 mg mL^{-1} OVA particles or a 1:1 water-in-oil emulsion of 1 mg mL^{-1} OVA protein in DPBS and IFA (25 μL per foot). Lymph nodes (side and leg) were taken 1 week later. Single-cell suspensions were prepared using a gentleMACS dissociator (Miltenyl Biotec). T cells were isolated using magnetic-activated cell sorting using an autoMACS cell sorter (Miltenyl Biotec).

T Cell Proliferation Assay. Suspensions of 3×10^5 APCs and 3×10^5 T cells were cultured. Particles were pulsed with serial dilutions of particles or free OVA ranging from 50 to 0.39 μg mL^{-1}. ^{3}H-Thymidine was added after ~70 h of incubation at 37 °C, 5% CO_2. ^{3}H-Thymidine incorporation was assessed using a beta counter 24 h later (*i.e.*, ~94 h incubation total). Data are representative for three independent experiments.

ELISPOT Assay. Suspensions of 3×10^5 APCs and 3×10^5 T cells were cultured onto IL-4 and IFN-γ ELISPOT plates (Millipore) in triplicate and restimulated with 2.5 μg of either OVA particles or free OVA. ELISPOT plates were developed according to the manufacturer's instructions after ~70 h of incubation at 37 °C, 5% CO_2. Data are representative for three independent experiments.

Immunization for Antibody Study. C57BL/6 mice, 6−8 weeks old, were immunized intraperitoneally with 25 μL of either 1 mg mL^{-1} OVA particles or a 1:1 water-in-oil emulsion of 1 mg mL^{-1} OVA protein in DPBS and IFA. After 21 days the mice were given a booster subcutaneous injection with the same antigens and then bled 10 days later. The collected sera were individually stored at −20 °C.

ELISA. Enzyme-linked immunosorbent assays were performed on sera from five mice in each group. OVA protein (10 μg mL^{-1}) in DPBS was used to coat wells of 96-well flat-bottom polystyrene EIA/RIA plates (Corning Costar) overnight at 4 °C. The coating solution was removed, and 5% (wt/vol) skim milk powder in PBS was added to block the remaining uncoated surface for 1 h at room temperature. Wells were then washed three times with PBS-T (0.01% Tween-20) and once with PBS. Double dilutions of subject sera in PBS containing 2.5% (wt/vol) skim milk powder from 1/12.5 to 1/1600 were added to wells and incubated overnight at 4 °C. Wells were washed three times with PBS-T and once with PBS and incubated with goat anti-mouse (2.5% skim milk/PBS) directed against total IgG (1/4000 dilution) for 1 h at room temperature. Wells were washed three

times with PBS-T and once with PBS, and bound antibody was detected by incubation with horseradish peroxidase-conjugated swine anti-goat (1/4000 dilution) for 1 h at room temperature. Wells were washed three times with PBS-T and once with PBS. Substrate, ABTS in 50 mM citric acid buffer containing 0.02% (v/v) hydrogen peroxide, was added. After incubation for approximately 1 h, optical density at 405 nm was measured using a Bio-Rad microplate reader, model 450.

Statistical Analysis. Statistical analysis was performed using Graphpad Prism v5.0c. ELISPOT and ELISA were analyzed using a one-way ANOVA and Bonferroni's multiple comparison test. T cell proliferation was analyzed using two-way ANOVA and Bonferroni post-tests.

Conflict of Interest: The authors declare no competing financial interest.

Acknowledgment. This work was supported by the Australian Research Council under the Australian Laureate Fellowship (F.C., FL120100030), Discovery Early Career Researcher Award (Y.Y., DE130100488), and the ARC Centre of Excellence in Convergent Bio-Nano Science and Technology (CE140100036) schemes, as well as the National Health and Medical Research Council Project Grant (APP1029878). K.T.G. acknowledges funding from the Australian Government through an International Postgraduate Research Scholarship and an Australian Postgraduate Award.

Supporting Information Available: Thiol characterization and intracellular degradation of o-OVA *versus* reduced o-OVA particles in RAW cells. Statistical analysis for T cell (proliferation and cytokine secretion) and antibody experiments found in Figures 7−9. ELISPOT experiment showing the number of IL-4- and IFN-γ-secreting T cells following immunization with PBS and IFA and stimulation with OVA particles or soluble OVA *ex vivo*. This material is available free of charge *via* the Internet at http://pubs.acs.org.

REFERENCES AND NOTES

1. Irvine, D. J.; Swartz, M. A.; Szeto, G. L. Engineering Synthetic Vaccines Using Cues from Natural Immunity. *Nat. Mater.* **2013**, *12*, 978–990.
2. DeMuth, P. C.; Min, Y. J.; Huang, B.; Kramer, J. A.; Miller, A. D.; Barouch, D. H.; Hammond, P. T.; Irvine, D. J. Polymer Multilayer Tattooing for Enhanced DNA Vaccination. *Nat. Mater.* **2013**, *12*, 367–376.
3. Leleux, J.; Roy, K. Micro and Nanoparticle-Based Delivery Systems for Vaccine Immunotherapy: An Immunological and Materials Perspective. *Adv. Healthcare Mater.* **2013**, *2*, 72–94.
4. De Koker, S.; Lambrecht, B. N.; Willart, M. A.; van Kooyk, Y.; Grooten, J.; Vervaet, C.; Remon, J. P.; De Geest, B. G. Designing Polymeric Particles for Antigen Delivery. *Chem. Soc. Rev.* **2011**, *40*, 320–339.
5. Smith, D. M.; Simon, J. K.; Baker, J. R. Applications of Nanotechnology for Immunology. *Nat. Rev. Immunol.* **2013**, *13*, 592–605.
6. DeMuth, P. C.; Moon, J. J.; Suh, H.; Hammond, P. T.; Irvine, D. J. Releasable Layer-by-Layer Assembly of Stabilized Lipid Nanocapsules on Microneedles for Enhanced Transcutaneous Vaccine Delivery. *ACS Nano* **2012**, *6*, 8041–8051.
7. Mody, K. T.; Popat, A.; Mahony, D.; Cavallaro, A. S.; Yu, C. Z.; Mitter, N. Mesoporous Silica Nanoparticles as Antigen Carriers and Adjuvants for Vaccine Delivery. *Nanoscale* **2013**, *5*, 5167–5179.
8. Tao, Y.; Ju, E. G.; Li, Z. H.; Ren, J. S.; Qu, X. G. Engineered CpG-Antigen Conjugates Protected Gold Nanoclusters as Smart Self-Vaccines for Enhanced Immune Response and Cell Imaging. *Adv. Funct. Mater.* **2014**, *24*, 1004–1010.
9. Phanse, Y.; Carrillo-Conde, B. R.; Ramer-Tait, A. E.; Broderick, S.; Kong, C. S.; Rajan, K.; Flick, R.; Mandell, R. B.; Narasimhan, B.; Wannemuehler, M. J. A Systems Approach to Designing Next Generation Vaccines: Combining Alpha-Galactose Modified Antigens with Nanoparticle Platforms. *Sci. Rep.* **2014**, *4*, 3775.
10. Rouas, N.; Christophe, S.; Housseau, F.; Bellet, D.; Guillet, J. G.; Bidart, J. M. Influence of Protein-Quaternary Structure on Antigen Processing. *J. Immunol.* **1993**, *150*, 782–792.
11. Glimcher, L. H.; Schroer, J. A.; Chan, C.; Shevach, E. M. Fine Specificity of Cloned Insulin-Specific T-Cell Hybridomas - Evidence Supporting a Role for Tertiary Conformation. *J. Immunol.* **1983**, *131*, 2868–2874.
12. Janssen, R.; Wauben, M. H. M.; Tommassen, J. Quaternary Structure of a Carrier Protein Influences Antigenicity and Immunogenicity of an Inserted T Cell Determinant. *Int. Immunol.* **1996**, *8*, 829–836.
13. Thai, R.; Moine, G.; Desmadril, M.; Servent, D.; Tarride, J. L.; Menez, A.; Leonetti, M. Antigen Stability Controls Antigen Presentation. *J. Biol. Chem.* **2004**, *279*, 50257–50266.
14. Ametani, A.; Sakurai, T.; Katakura, Y.; Kuhara, S.; Hirakawa, H.; Hosoi, T.; Dosako, S. I.; Kaminogawa, S. Amino Acid Residue Substitution at T-Cell Determinant-Flanking Sites in Beta-Lactoglobulin Modulates Antigen Presentation to T Cells through Subtle Conformational Change. *Biosci., Biotechnol., Biochem.* **2003**, *67*, 1507–1514.
15. Ohkuri, T.; Nagatomo, S.; Oda, K.; So, T.; Imoto, T.; Ueda, T. A Protein's Conformational Stability is an Immunologically Dominant Factor: Evidence that Free-Energy Barriers for Protein Unfolding Limit the Immunogenicity of Foreign Proteins. *J. Immunol.* **2010**, *185*, 4199–4205.
16. So, T.; Ito, H.; Koga, T.; Watanabe, S.; Ueda, T.; Imoto, T. Depression of T-Cell Epitope Generation by Stabilizing Hen Lysozyme. *J. Biol. Chem.* **1997**, *272*, 32136–32140.
17. Prato, S.; Fleming, J.; Schmidt, C. W.; Corradin, G.; Lopez, J. A. Cross-Presentation of a Human Malaria CTL Epitope Is Conformation Dependent. *Mol. Immunol.* **2006**, *43*, 2031–2036.
18. Carmicle, S.; Dai, G. X.; Steede, N. K.; Landry, S. J. Proteolytic Sensitivity and Helper T-Cell Epitope Immunodominance Associated with the Mobile Loop in Hsp10s. *J. Biol. Chem.* **2002**, *277*, 155–160.
19. Schneider, S. C.; Ohmen, J.; Fosdick, L.; Gladstone, B.; Guo, J.; Ametani, A.; Sercarz, E. E.; Deng, H. K. Cutting Edge: Introduction of an Endopeptidase Cleavage Motif into a Determinant Flanking Region of Hen Egg Lysozyme Results in Enhanced T Cell Determinant Display. *J. Immunol.* **2000**, *165*, 20–23.
20. Antoniou, A. N.; Blackwood, S. L.; Mazzeo, D.; Watts, C. Control of Antigen Presentation by a Single Protease Cleavage Site. *Immunity* **2000**, *12*, 391–398.
21. Zhang, L.; Liu, W. G.; Lin, L.; Chen, D. Y.; Stenzel, M. H. Degradable Disulfide Core-Cross-Linked Micelles as a Drug Delivery System Prepared from Vinyl Functionalized Nucleosides *via* the RAFT Process. *Biomacromolecules* **2008**, *9*, 3321–3331.
22. Cui, J.; De Rose, R.; Best, J. P.; Johnston, A. P. R.; Alcantara, S.; Liang, K.; Such, G. K.; Kent, S. J.; Caruso, F. Mechanically Tunable, Self-Adjuvanting Nanoengineered Polypeptide Particles. *Adv. Mater.* **2013**, *25*, 3468–3472.
23. Bundy, B. C.; Swartz, J. R. Efficient Disulfide Bond Formation in Virus-like Particles. *J. Biotechnol.* **2011**, *154*, 230–239.
24. Chong, S.-F.; Sexton, A.; De Rose, R.; Kent, S. J.; Zelikin, A. N.; Caruso, F. A Paradigm for Peptide Vaccine Delivery Using Viral Epitopes Encapsulated in Degradable Polymer Hydrogel Capsules. *Biomaterials* **2009**, *30*, 5178–5186.
25. Sexton, A.; Whitney, P. G.; Chong, S.-F.; Zelikin, A. N.; Johnston, A. P. R.; De Rose, R.; Brooks, A. G.; Caruso, F.; Kent, S. J. A Protective Vaccine Delivery System for *in Vivo* T Cell Stimulation Using Nanoengineered Polymer Hydrogel Capsules. *ACS Nano* **2009**, *3*, 3391–3400.
26. De Rose, R.; Zelikin, A. N.; Johnston, A. P. R.; Sexton, A.; Chong, S.-F.; Cortez, C.; Mulholland, W.; Caruso, F.; Kent, S. J. Binding, Internalization, and Antigen Presentation of Vaccine-Loaded Nanoengineered Capsules in Blood. *Adv. Mater.* **2008**, *20*, 4698–4703.
27. Cui, J.; van Koeverden, M. P.; Müllner, M.; Kempe, K.; Caruso, F. Emerging Methods for the Fabrication of Polymer Capsules. *Adv. Colloid Interface Sci.* **2014**, *207*, 14–31.
28. Smith, M. T.; Hawes, A. K.; Bundy, B. C. Reengineering Viruses and Virus-like Particles through Chemical

Functionalization Strategies. *Curr. Opin. Biotechnol.* **2013**, *24*, 620–626.
29. Pejawar-Gaddy, S.; Rajawat, Y.; Hilioti, Z.; Xue, J.; Gaddy, D. F.; Finn, O. J.; Viscidi, R. P.; Bossis, I. Generation of a Tumor Vaccine Candidate Based on Conjugation of a MUC1 Peptide to Polyionic Papillomavirus Virus-like Particles. *Cancer Immunol. Immun.* **2010**, *59*, 1685–1696.
30. Martner, A.; Aurelius, J.; Rydstrom, A.; Hellstrand, K.; Thoren, F. B. Redox Remodeling by Dendritic Cells Protects Antigen-Specific T Cells against Oxidative Stress. *J. Immunol.* **2011**, *187*, 6243–6248.
31. Wang, Y.; Yu, A.; Caruso, F. Nanoporous Polyelectrolyte Spheres Prepared by Sequentially Coating Sacrificial Mesoporous Silica Spheres. *Angew. Chem., Int. Ed.* **2005**, *44*, 2888–2892.
32. Wang, Y.; Price, A. D.; Caruso, F. Nanoporous Colloids: Building Blocks for a New Generation of Structured Materials. *J. Mater. Chem.* **2009**, *19*, 6451–6464.
33. Cui, J.; Yan, Y.; Wang, Y.; Caruso, F. Templated Assembly of pH-Labile Polymer-Drug Particles for Intracellular Drug Delivery. *Adv. Funct. Mater.* **2012**, *22*, 4718–4723.
34. Huntington, J. A.; Stein, P. E. Structure and Properties of Ovalbumin. *J. Chromatogr. B* **2001**, *756*, 189–198.
35. Boncel, S.; Walczak, K. Novel Acyclic Amide-Conjugated Nucleosides and Their Analogues. *Nucleosides, Nucleotides Nucleic Acids* **2009**, *28*, 103–117.
36. Narayan, M.; Welker, E.; Wedemeyer, W. J.; Scheraga, H. A. Oxidative Folding of Proteins. *Acc. Chem. Res.* **2000**, *33*, 805–812.
37. Takahashi, N.; Koseki, T.; Doi, E.; Hirose, M. Role of an Intrachain Disulfide Bond in the Conformation and Stability of Ovalbumin. *J. Biochem.* **1991**, *109*, 846–851.
38. Aderem, A.; Underhill, D. M. Mechanisms of Phagocytosis in Macrophages. *Annu. Rev. Immunol.* **1999**, *17*, 593–623.
39. Houde, M.; Bertholet, S.; Gagnon, E.; Brunet, S.; Goyette, G.; Laplante, A.; Princiotta, M. F.; Thibault, P.; Sacks, D.; Desjardins, M. Phagosomes Are Competent Organelles for Antigen Cross-Presentation. *Nature* **2003**, *425*, 402–406.
40. Watts, C. Phagosome Neutrality in Host Defense. *Cell* **2006**, *126*, 17–19.
41. Kastl, L.; Sasse, D.; Wulf, V.; Hartmann, R.; Mircheski, J.; Ranke, C.; Carregal-Romero, S.; Martinez-Lopez, J. A.; Fernandez-Chacon, R.; Parak, W. J.; *et al.* Multiple Internalization Pathways of Polyelectrolyte Multilayer Capsules into Mammalian Cells. *ACS Nano* **2013**, *7*, 6605–6618.
42. Miksa, M.; Kornura, H.; Wu, R. Q.; Shah, K. G.; Wang, P. A Novel Method to Determine the Engulfment of Apoptotic Cells by Macrophages Using pHrodo Succinimidyl Ester. *J. Immunol. Methods* **2009**, *342*, 71–77.
43. Albanese, A.; Tang, P. S.; Chan, W. C. W. The Effect of Nanoparticle Size, Shape, and Surface Chemistry on Biological Systems. *Annu. Rev. Biomed. Eng.* **2012**, *14*, 1–16.
44. Mottram, P. L.; Leong, D.; Crimeen-Irwin, B.; Gloster, S.; Xiang, S. D.; Meanger, J.; Ghildyal, R.; Vardaxis, N.; Plebanski, M. Type 1 and 2 Immunity Following Vaccination Is Influenced by Nanoparticle Size: Formulation of a Model Vaccine for Respiratory Syncytial Virus. *Mol. Pharmaceutics* **2007**, *4*, 73–84.
45. Foged, C.; Brodin, B.; Frokjaer, S.; Sundblad, A. Particle Size and Surface Charge Affect Particle Uptake by Human Dendritic Cells in an *in Vitro* Model. *Int. J. Pharm.* **2005**, *298*, 315–322.
46. Streicher, H. Z.; Berkower, I. J.; Busch, M.; Gurd, F. R. N.; Berzofsky, J. A. Antigen Conformation Determines Processing Requirements for T-Cell Activation. *Proc. Natl. Acad. Sci. U.S.A.* **1984**, *81*, 6831–6835.
47. Collins, D. S.; Unanue, E. R.; Harding, C. V. Reduction of Disulfide Bonds within Lysosomes is a Key Step in Antigen Processing. *J. Immunol.* **1991**, *147*, 4054–4059.
48. Foster, E. S.; Kimber, I.; Dearman, R. J. Relationship between Protein Digestibility and Allergenicity: Comparisons of Pepsin and Cathepsin. *Toxicology* **2013**, *309*, 30–38.
49. De Geest, B. G.; Willart, M. A.; Lambrecht, B. N.; Pollard, C.; Vervaet, C.; Remon, J. P.; Grooten, J.; De Koker, S. Surface-Engineered Polyelectrolyte Multilayer Capsules: Synthetic Vaccines Mimicking Microbial Structure and Function. *Angew. Chem., Int. Ed.* **2012**, *51*, 3862–3866.
50. De Koker, S.; De Geest, B. G.; Singh, S. K.; De Rycke, R.; Naessens, T.; Van Kooyk, Y.; Demeester, J.; De Smedt, S. C.; Grooten, J. Polyelectrolyte Microcapsules as Antigen Delivery Vehicles to Dendritic Cells: Uptake, Processing, and Cross-Presentation of Encapsulated Antigens. *Angew. Chem., Int. Ed.* **2009**, *48*, 8485–8489.
51. Howland, S. W.; Wittrup, K. D. Antigen Release Kinetics in the Phagosome Are Critical to Cross-Presentation Efficiency. *J. Immunol.* **2008**, *180*, 1576–1583.
52. Broaders, K. E.; Cohen, J. A.; Beaudette, T. T.; Bachelder, E. M.; Frechet, J. M. J. Acetalated Dextran Is a Chemically and Biologically Tunable Material for Particulate Immunotherapy. *Proc. Natl. Acad. Sci. U.S.A.* **2009**, *106*, 5497–5502.
53. Wang, J.-G.; Zhou, H.-J.; Sun, P.-C.; Ding, D.-T.; Chen, T.-H. Hollow Carved Single-Crystal Mesoporous Silica Templated by Mesomorphous Polyelectrolyte-Surfactant Complexes. *Chem. Mater.* **2010**, *22*, 3829–3831.
54. Shapero, K.; Fenaroli, F.; Lynch, I.; Cottell, D. C.; Salvati, A.; Dawson, K. A. Time and Space Resolved Uptake Study of Silica Nanoparticles by Human Cells. *Mol. Biosyst.* **2011**, *7*, 371–378.
55. Wong, D. M.; Tam, V.; Lam, R.; Walsh, K. A.; Tatarczuch, L.; Pagel, C. N.; Reynolds, E. C.; O'Brien-Simpson, N. M.; Mackie, E. J.; Pike, R. N. Protease-Activated Receptor 2 Has Pivotal Roles in Cellular Mechanisms Involved in Experimental Periodontitis. *Infect. Immun.* **2010**, *78*, 629–638.